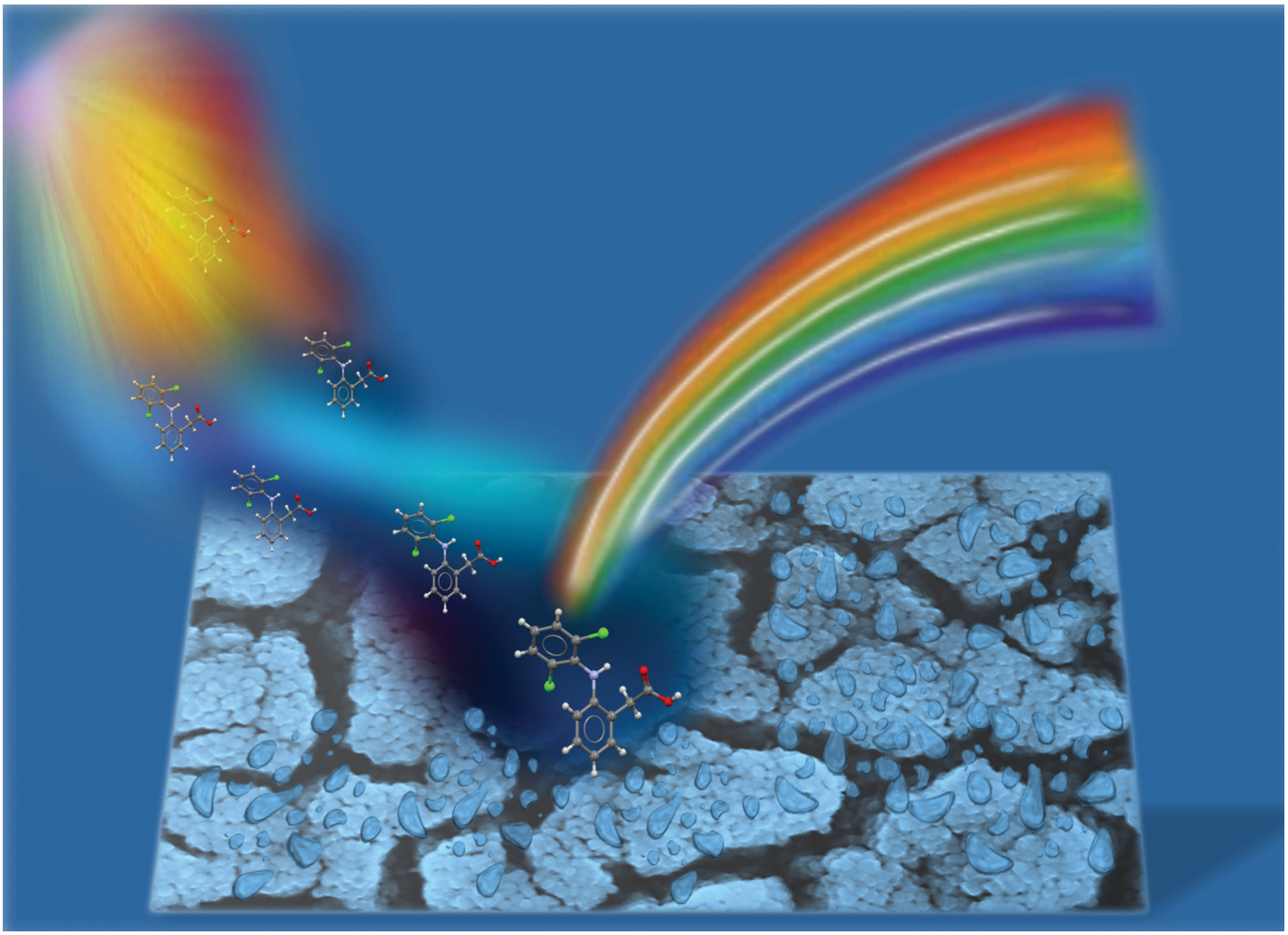

Showcasing research from Padova University - Department of Chemical Sciences, CNR-ICMATE and INSTM, Padova, Italy, in collaboration with the University of Ljubljana and National Institute of Chemistry, Ljubljana, Slovenia

Controllable properties of NiO nanostructures fabricated by plasma assisted-chemical vapor deposition

Plasma assisted-vapor deposition at temperatures as low as 100 °C yielded NiO nanostructures with features tuneable as a function of the process duration. In particular, tailoring of the grain dimensions and deposit thickness affects both the system wetting behavior and photodegradation efficiency towards aqueous diclofenac, a persistent pharmaceutical pollutant.

As featured in:

See Chiara Maccato *et al.*, *Chem. Commun.*, 2025, **61**, 2945.

ROYAL SOCIETY OF CHEMISTRY

rsc.li/chemcomm

Registered charity number: 207890

ChemComm

COMMUNICATION

View Article Online
View Journal | View Issue

Cite this: *Chem. Commun.*, 2025, **61**, 2945

Received 13th December 2024,
Accepted 13th January 2025

DOI: 10.1039/d4cc06548d

rsc.li/chemcomm

Controllable properties of NiO nanostructures fabricated by plasma assisted-chemical vapor deposition†

Davide Barreca, [a] Enrico Scattolin, [b] Chiara Maccato, *[ab] Alberto Gasparotto, [ab] Lorenzo Signorin, [b] Naida El Habra, [ae] Andraž Šuligoj, [cd] Urška Lavrenčič Štangar [d] and Gian Andrea Rizzi [ab]

An original plasma assisted vapor phase route is proposed for the low-temperature fabrication of supported NiO nanostructures on conductive glasses. The sole deposition time variation enables to tailor material properties, modulating, in turn, the system wettability and functional performances in the photodegradation of recalcitrant pollutants.

Thin films and nanomaterials of nickel(II) oxide (NiO), a p-type pluripotent semiconductor featuring a good chemical stability, stand as appealing candidates for a plethora of technological applications, encompassing solar cells,[1–3] electrochromic devices,[4–7] gas sensors,[8–10] and heterogeneous (photo)catalysts for various processes, including hydrogen production, oxygen evolution in water splitting, and degradation of aqueous organic pollutants.[11–16] In addition, NiO systems are attractive as hydrophobic coatings for protection against corrosion, offering also self-cleaning, anti-fouling, and frost-prevention properties.[17,18]

The aforementioned applications have significantly stimulated research activities aimed at the preparation of NiO films/nanosystems by different techniques, including sputtering,[2,7,9] evaporation,[10] electrodeposition,[16,17] hydrothermal routes,[11] sol–gel,[1,3] spray pyrolysis,[6,8] atomic layer deposition (ALD)[5,14] and chemical vapor deposition (CVD),[4,12,15,19] a potentially scalable route featuring manifold concurrent benefits. In this regard, plasma-assisted processes are appealing preparation strategies for multi-functional nanoarchitectures, owing to the unique features and activation mechanisms of non-equilibrium plasmas that enable deposition at low temperatures even on thermally labile supports.[20] Nevertheless, to the best of our knowledge, only two reports on the plasma assisted-CVD of NiO films are available in the literature so far.[13,21]

Recently, we have proposed variously substituted diketonate–diamine Ni(II) complexes as valuable precursors for the CVD of NiO films.[19,22] Herein, we report for the first time on the plasma assisted-chemical vapor deposition (PA-CVD) of Ni(II) oxide nanosystems from one of these precursors (see the ESI†). The target systems were grown at a temperature of 100 °C, much lower than those adopted in previous plasma-assisted vapor phase syntheses,[13,14,21] on fluorine-doped tin oxide (FTO), focusing on the influence exerted by the deposition time (10, 30, 60, 90 min) on material chemico-physical characteristics. The latter were investigated by means of forefront complementary techniques, including ultraviolet photoelectron spectroscopy (UPS) and reflection electron energy loss spectroscopy (REELS), used for the first time on similar systems in conjunction with X-ray photoelectron spectroscopy (XPS). In fact, REELS can probe the presence of hydrogen,[23] which, though being elusive, may directly affect the system behavior. In addition, functional properties were investigated with particular regard to the system wettability, by measurements of water contact angle (WCA) values.[18,24] Attention was also dedicated for the first time, as a proof-of-concept, to assessing material activity in the photodegradation of aqueous diclofenac {DCF; 2-[2-(2,6-dichloroanilino)phenyl]acetic acid},[22] a nonsteroidal anti-inflammatory drug, as a representative persistent pharmaceutical pollutant.[25]

Fig. 1a (see also Fig. S1, ESI†) reports X-ray diffraction (XRD) patterns for NiO samples grown for different durations. Besides FTO reflections, all diffractograms clearly showed three signals ascribed to (111), (200) and (220) crystallographic planes of cubic NiO.[19,26] The analysis of relative peak intensities indicated that crystallites were preferentially oriented along [111] and [220] directions (see also Fig. S2, ESI†). Additional efforts were dedicated to the analysis of material composition by means of XPS (see also Fig. S3–S5 and Table S1, ESI†). Ni2p

[a] *CNR-ICMATE and INSTM, Department of Chemical Sciences, Padova University Via Marzolo 1, 35131 Padova, Italy*
[b] *Department of Chemical Sciences, Padova University and INSTM, 35131 Padova, Italy. E-mail: chiara.maccato@unipd.it*
[c] *National Institute of Chemistry, Ljubljana SI-1000, Slovenia*
[d] *Faculty of Chemistry and Chemical Technology, University of Ljubljana, Ljubljana SI-1000, Slovenia*
[e] *CNR-ICMATE, 35127 Padova, Italy*

† Electronic supplementary information (ESI) available. See DOI: https://doi.org/10.1039/d4cc06548d

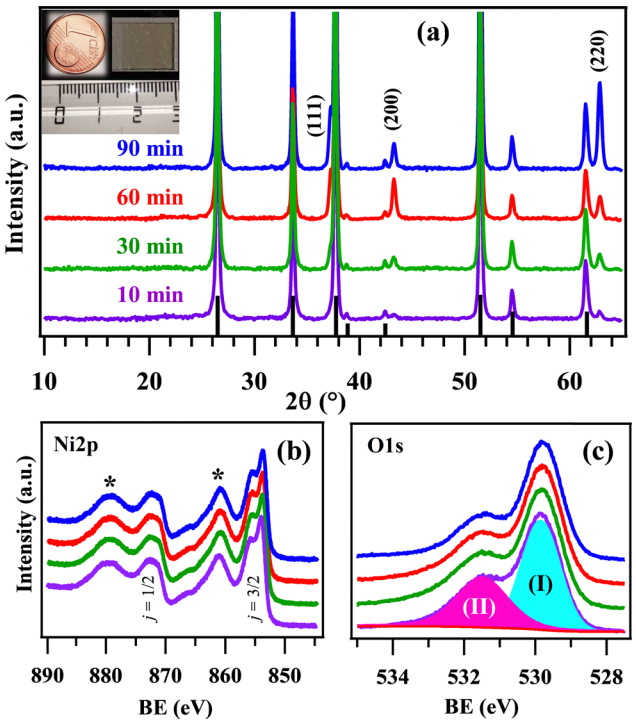

Fig. 1 (a) XRD patterns of NiO deposits obtained at different deposition times. Reflections from the FTO substrate are marked by vertical black bars. Inset: Photograph of a specimen obtained for a process duration of 90 min. Ni2p (b) and O1s (c) photoelectron peaks for the target specimens.

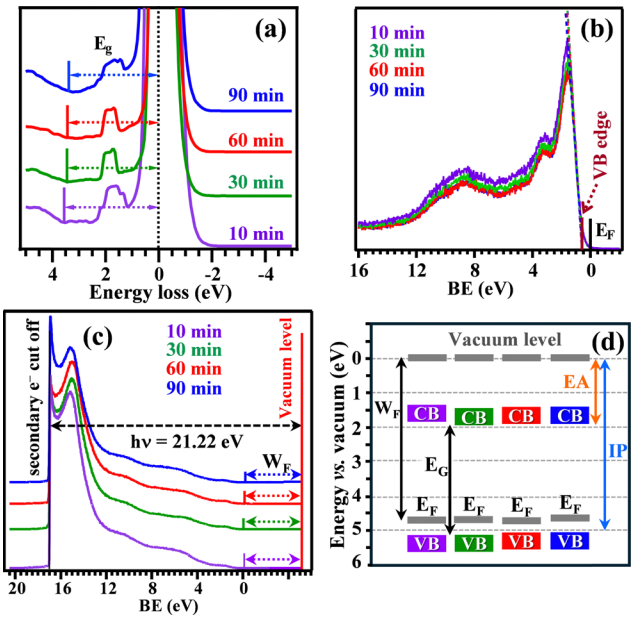

Fig. 2 (a) REELS spectra, (b) XPS valence bands, (c) He(I) UPS valence bands, and (d) energy level positions for the different systems with respect to the vacuum level (E_F = Fermi level energy; E_G = band gap; W_F = work function; CB = conduction band; VB = valence band; EA = electron affinity; IP = ionization potential).

peaks position and shape (Fig. 1b), featuring a peculiar multiplet structure with satellite signals at energy ≈6 eV higher than the main spin–orbit components, were in line with previous studies on Ni(II) oxide.[11,19] The presence of NiO was also supported by the O1s peak, exhibiting a component at ≈529.9 eV [(I) in Fig. 1c], attributable to NiO lattice oxygen,[12,27] whereas band (II) at 531.5 eV (Table S2, ESI†) was mainly due to the concurrence of –OH groups and atmospheric oxygen adsorbed onto O defect sites.[19,28] The presence of tin from the FTO substrate (Fig. S6, ESI†), with a progressively lower content upon increasing the deposition time, was also observed. As demonstrated by morphological analyses (see Fig. 3 and below), this trend can be ascribed to the progressive deposit thickness increase for longer PA-CVD durations, gradually hindering the underlying SnO_2 detection. Additional information on the electronic properties of the target systems was obtained by REELS and valence band spectra. For all samples, the recorded REELS spectra (Fig. 2a) featured an intense peak at zero energy loss due to elastically scattered electrons, and a signal below 2 eV due to scattering collisions with hydrogen atoms,[23] whose content can be envisaged to be qualitatively higher at lower deposition times. An increase in the PA-CVD process duration resulted in a modest decrease of the measured energy gap from 3.6 to 3.3 eV (Table S3, ESI†), the latter value being in line with that reported for bulk NiO.[19] The separation of the valence band edge from the Fermi level energy (see Fig. 2b and Table S3, ESI;† values are in good agreement with the p-type character of NiO[19]) underwent a slight decrease upon going from the 10 min sample to the 90 min one. Finally, the analysis of UPS valence band spectra (Fig. 2c), in conjunction with the other data, enabled to obtain the parameters marked in Fig. 2d and reported in Table S3, ESI.† The work function values were all very close to 4.7 eV, in accordance with the literature.[29,30] A detailed inspection of the obtained data revealed only minor differences in the electronic properties of the target systems, suggesting thus that their functional properties were mainly affected by the actual material morphology (see below).

Field emission-scanning electron microscopy (FE-SEM) images of the target NiO specimens are reported in Fig. 3a–d. A careful micrograph inspection showed that a process duration of 10 min (Fig. 3a) resulted in a conformal coverage of the FTO substrate by the NiO deposit. An increase of the PA-CVD process duration, thanks to the synergy between material deposition and modification induced by the used plasmas,[20] resulted in the progressive development of a nanocolumnar, open area morphology, a feature particularly evident for the longest deposition time (Fig. 3d). These results suggested the occurrence of a hybrid 2D–3D growth mode, likely favored by the inherently rough surface of the used FTO supports.[31,32] The average deposit thickness linearly increased with the corresponding deposition time (Fig. 3e), indicating the possibility of exerting a fine control of this parameter and of the related properties by simple modulations of the process duration. The surface topography of the samples, investigated by atomic force microscopy (AFM) (see Fig. 3f and Fig. S7, ESI†), did not show a significant variation in the root-mean-square (RMS) roughness as a function of deposition time. In fact, the system

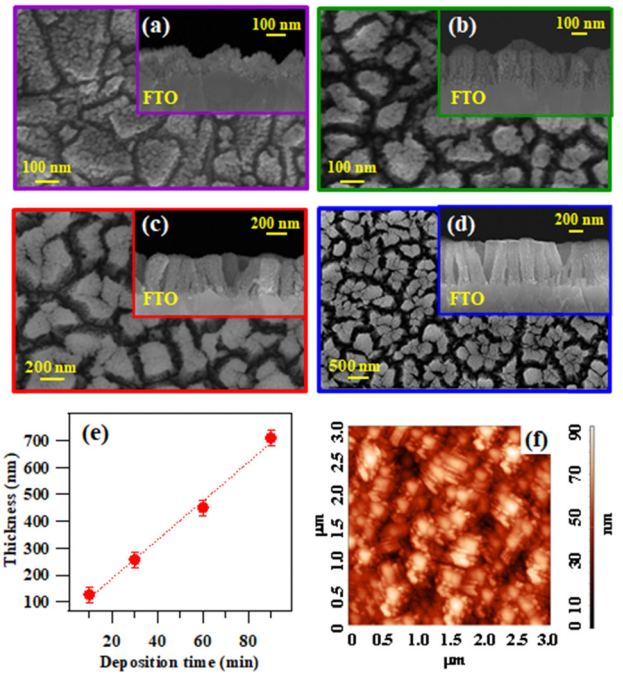

Fig. 3 (a)–(d) Representative plane-view and cross-sectional (inset) FE-SEM images for NiO specimens supported on FTO, obtained at different deposition times: (a) 10 min; (b) 30 min; (c) 60 min; (d) 90 min. (e) Dependence of the deposit thickness on deposition time. (f) AFM micrograph for a NiO specimen obtained for 10 min (RMS roughness ≈16 nm).

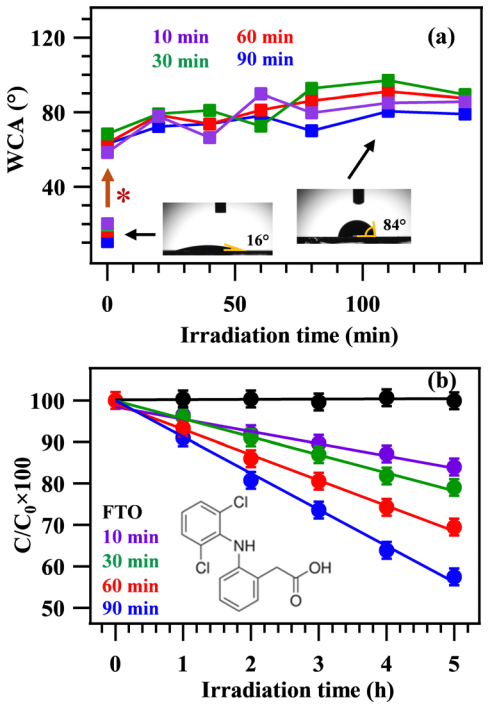

Fig. 4 (a) Wetting behavior of NiO specimens: water contact angle evolution as a function of irradiation time. The brown arrow marked by (*) corresponds to 24 days of exposure to laboratory atmosphere. Inset: Photographs of H_2O droplets on a sample obtained for a process duration of 90 min at different illumination stages. (b) Photocatalytic performances in diclofenac (inset) degradation for NiO samples obtained at different deposition times. The used setup enables the test of relatively low surface-to-volume ratio samples, hence the surface was saturated with DCF molecules, resulting in an apparent zero-order degradation kinetics. The bare FTO substrate did not show any activity, and hence its influence can be excluded.

morphology prevents from a successful probing of the materials in their real depth-profile, returning an almost constant RMS value of ≈16 nm.

The attention was subsequently dedicated to investigating the system wetting properties as a function of PA-CVD growth duration by measuring WCA values (see Fig. 4a and Fig. S8, ESI†). Specimens deposited for 10, 30, 60, and 90 min showed pristine WCA values of 20.0, 19.5, 16.2, and 10.6°, respectively. These values showcased a higher hydrophilic character for thicker NiO systems, offering a larger surface area to the water droplet wetting the surface. A significant WCA increase up to ≈60–70° was observed after 24 days of exposure to laboratory air (Fig. 4a). This result, in line with those obtained for nickel micro-nano cones array,[33] may be related to the adsorption of hydrocarbons on the target material surface.[34] Concurrent issues accounting for this behavior can be associated to: (i) the existence of oxygen vacancies (as evidenced by XPS analyses, see above) promoting a progressive O_2 adsorption, which, in turn, can contribute to the observed hydrophobicity; (ii) the presence of surface CF_x groups (Fig. S5, ESI†), resulting in the maintenance of the hydrophobic behavior upon irradiation.[35,36] In fact, during the subsequent UVA light illumination, only a slight WCA variation occurred during the first 20 min, and the measured WCAs remained in the ≈80–90° range for the whole experiment duration (140 min; Fig. 4a). These results evidenced that the obtained materials maintained their hydrophobic characteristics and did not promote photodegradation processes of surface solid contaminants, as confirmed by tests carried out using methyl stearate (see the ESI† and Fig. S9). However, as the NiO deposit thickening contributed to a better wettability and to a band gap decrease to 3.3 eV (deposition time of 90 min, Table S3, ESI†), additional efforts were dedicated to assessing the system photocatalytic activity in the degradation of DCF, whose initial adsorption might be possibly favoured by the hydrophobic surface nature.[37] The obtained results (Fig. 4b) showed a noticeable activity, which underwent a progressive increase with the deposit thickness (see Fig. 3e). Interestingly, the trend in DCF degradation followed the trend of pristine hydrophilicity, highlighting that the most hydrophilic sample (the one with a PA-CVD duration of 90 min) produced the fastest DCF degradation (see also Table S4, ESI†). Although NiO as such suffers from a relatively fast recombination of photogenerated charge carriers,[38] the presence of the FTO substrate (n-type) below NiO (p-type) enables electron injection into FTO, whereas holes accumulate on NiO,[39] accounting thus for DCF degradation. It is worthwhile noticing that thicker deposits feature the occurrence of higher columns (Fig. 3), as well as of larger NiO grains atop the columns themselves (see Fig. S10, ESI†). These issues foster an increased UV light absorption (see Fig. S11, ESI†), leading to a more efficient charge carrier generation and, ultimately, to a faster DCF degradation in the case of the 90 min specimen. An

additional contributing effect can be related to the higher active area of materials obtained for longer PA-CVD process durations.

In summary, phase-pure NiO supported nanostructures were successfully fabricated *via* plasma assisted-CVD on glassy substrates at temperatures of 100 °C, the lowest ever reported so far in similar processes. Modulation of the sole process duration enabled to tailor material morphology, with particular regard to grain dimensions and deposit thickness. These features directly affected material properties in terms of wettability and photodegradation efficiency of aqueous diclofenac, a persistent pharmaceutical product. This work demonstrates an amenable and straightforward strategy for the preparation of NiO nanostructures, that can be conveniently extended even to thermally labile substrates. In perspective, the system surface hydrophobicity can be exploited in the design of catalysts with improved activity and selectivity. Furthermore, the flexible control over thickness and morphology of NiO systems renders them interesting candidates for additional photoactivated end-uses, including water splitting to green hydrogen. Efforts in this direction are already in progress.

Davide Barreca: conceptualization, investigation, methodology, writing – original draft. Enrico Scattolin: data curation, software, formal analysis. Chiara Maccato: vision, formal analysis, project administration, writing – review & editing, funding acquisition. Alberto Gasparotto: supervision, methodology, project administration, writing – review & editing. Lorenzo Signorin: methodology, validation. Naida El Habra: vision, data curation. Andraž Šuligoj: investigation, methodology, writing – original draft. Urška Lavrenčič Štangar: supervision, project administration. Gian Andrea Rizzi: conceptualization, software, supervision, writing – review & editing.

Padova University (P-DiSC#02BIRD2023-UNIPD RIGENERA), CNR (Progetti di Ricerca @CNR-avviso 2020-ASSIST), PRIN 2022474YE8 (SCI-TROPHY project), and ARIS (P1-0134 core funding) assisted financially the work.

Data availability

The data supporting this article have been included as part of the ESI.†

Conflicts of interest

There are no conflicts to declare.

Notes and references

1 M. Rajesh, K. Vengatesan, M. H. Aly, R. Sitharthan, S. S. Dhanabalan and M. Karthikeyan, *Opt. Quantum Electron.*, 2023, **55**, 1167.
2 C. Aivalioti, E. G. Manidakis, N. T. Pelekanos, M. Androulidaki, K. Tsagaraki, Z. Viskadourakis, E. Spanakis and E. Aperathitis, *Thin Solid Films*, 2023, **778**, 139910.
3 Q. S. Jiang, Y. Wu, Z. Xie, M. Wei, Y. Zhao, X. Yang, W. Xun, S. Cao and C. Wang, *Mater. Today Commun.*, 2023, **35**, 106401.
4 M. Z. Sialvi, R. J. Mortimer, G. D. Wilcox, A. M. Teridi, T. S. Varley, K. G. U. Wijayantha and C. A. Kirk, *ACS Appl. Mater. Interfaces*, 2013, **5**, 5675–5682.
5 X. Su, Z. Tu, L. Ji, H. Wu, H. Xu and C. Liu, *J. Vac. Sci. Technol., A*, 2023, **41**, 062407.
6 E. A. Khera, H. Ullah, F. Hussain, S. Abubakar, A. Majeed, I. Tabssum, Z. Batool, A. Nazir and G. Gilanie, *ChemistrySelect*, 2023, **8**, e20230232.
7 Y. Tang, H. Shen, T. Wang, S. Peng, K. Jin, Q. Qian, G. Li and Z. Gan, *Thin Solid Films*, 2023, **769**, 139754.
8 K. Rajesh, N. Pothukanuri and M. V. R. Reddy, *Chem. Phys. Impact*, 2024, **8**, 100397.
9 S. Srivastava, C. Dwivedi, A. Yadav, A. Kumar, G. Gupta and P. Singh, *Mater. Lett.*, 2023, **351**, 135040.
10 D. Dastan, K. Shan, A. Jafari, T. Marszalek, M. K. A. Mohammed, L. Tao, Z. Shi, Y. Chen, X.-T. Yin, N. D. Alharbi, F. Gity, S. Asgary, M. Hatamvand and L. Ansari, *Mater. Sci. Semicond. Process.*, 2023, **154**, 107232.
11 N. Kitchamsetti, M. S. Ramteke, S. R. Rondiya, S. R. Mulani, M. S. Patil, R. W. Cross, N. Y. Dzade and R. S. Devan, *J. Alloys Compd.*, 2021, **855**, 157337.
12 D. Zywitzki, D. H. Taffa, L. Lamkowski, M. Winter, D. Rogalla, M. Wark and A. Devi, *Inorg. Chem.*, 2020, **59**, 10059–10070.
13 N. Weidler, J. Schuch, F. Knaus, P. Stenner, S. Hoch, A. Maljusch, R. Schäfer, B. Kaiser and W. Jaegermann, *J. Phys. Chem. C*, 2017, **121**, 6455–6463.
14 S. Haghverdi Khamene, C. van Helvoirt, M. N. Tsampas and M. Creatore, *J. Phys. Chem. C*, 2023, **127**, 22570–22582.
15 K. Munawar, M. A. Mansoor, R. Naeem, M. Rizwan, M. S. Ahmad, T. Zaharinie, M. N. M. Zubir and Z. Aspanut, *Thin Solid Films*, 2023, **782**, 140031.
16 H. Chen, D. Ge, J. Chen, R. Li, X. Zhang, T. Yu, Y. Wang and S. Song, *Chem. Commun.*, 2020, **56**, 10529–10532.
17 A. Bahramian, M. Eyraud, F. Vacandio, V. Hornebecq, T. Djenizian and P. Knauth, *J. Appl. Electrochem.*, 2019, **49**, 621–629.
18 K. Liu, M. Vuckovac, M. Latikka, T. Huhtamäki and R. H. A. Ras, *Science*, 2019, **363**, 1147–1148.
19 M. Benedet, C. Maccato, G. Pagot, C. Invernizzi, C. Sada, V. Di Noto, G. A. Rizzi, E. Fois, G. Tabacchi and D. Barreca, *J. Phys. Chem. C*, 2023, **127**, 22304–22314.
20 A. Gasparotto, D. Barreca, D. Bekermann, A. Devi, R. A. Fischer, C. Maccato and E. Tondello, *J. Nanosci. Nanotechnol.*, 2011, **11**, 8206–8213.
21 M. Chandrakala, S. Raj Bharath, T. Maiyalagan and S. Arockiasamy, *Mater. Chem. Phys.*, 2017, **201**, 344–353.
22 M. Benedet, D. Barreca, E. Fois, R. Seraglia, G. Tabacchi, M. Roverso, G. Pagot, C. Invernizzi, A. Gasparotto, A. A. Heidecker, A. Pöthig, E. Callone, S. Dirè, S. Bogialli, V. Di Noto and C. Maccato, *Dalton Trans.*, 2023, **52**, 10677–10688.
23 S. D. Nehate, A. K. Saikumar and K. B. Sundaram, *Coatings*, 2021, **11**, 196.
24 D. Barreca and C. Maccato, *CrystEngComm*, 2023, **25**, 3968–3987.
25 N. Aghababaei, M. Abdouss, H. Hosseini-Monfared and F. Ghanbari, *J. Environ. Chem. Eng.*, 2023, **11**, 110477.
26 Pattern no 00-0047-1049, JCPDS, 2000.
27 G. Pagot, M. Benedet, C. Maccato, D. Barreca and V. Di Noto, *Surf. Sci. Spectra*, 2023, **30**, 024028.
28 D. Barreca, F. Gri, A. Gasparotto, G. Carraro, L. Bigiani, T. Altantzis, B. Žener, U. Lavrenčič Štangar, B. Alessi, D. B. Padmanaban, D. Mariotti and C. Maccato, *Nanoscale*, 2019, **11**, 98–108.
29 Y. Zhang, J. Zuo, P. Li, Y. Gao, W. He and Z. Zheng, *Physica E*, 2019, **111**, 75–78.
30 Y. Cheng, S. Lu, W. Xu, R. Boukherroub, S. Szunerits and W. Liang, *J. Alloys Compd.*, 2017, **723**, 225–236.
31 J. E. Prieto and I. Markov, *Surf. Sci.*, 2017, **664**, 172–184.
32 A. Baskaran and P. Smereka, *J. Appl. Phys.*, 2012, **111**, 044321.
33 W. Geng, A. Hu and M. Li, *Appl. Surf. Sci.*, 2012, **263**, 821–824.
34 J. Bae, I. A. Samek, P. C. Stair and R. Q. Snurr, *Langmuir*, 2019, **35**, 5762–5769.
35 G. Qi, X. Liu, C. Li, C. Wang and Z. Yuan, *Angew. Chem., Int. Ed.*, 2019, **58**, 17406–17411.
36 P. Dimitrakellis and E. Gogolides, *Adv. Colloid Interface Sci.*, 2018, **254**, 1–21.
37 N. Suriyanon, P. Punyapalakul and C. Ngamcharussrivichai, *Chem. Eng. J.*, 2013, **214**, 208–218.
38 T. Munawar, S. Fatima, M. S. Nadeem, F. Mukhtar, U. A. Akbar, A. S. Hakeem and F. Iqbal, *J. Mater. Sci.: Mater. Electron.*, 2023, **34**, 687.
39 B. Saha, K. Sarkar, A. Bera, K. Deb and R. Thapa, *Appl. Surf. Sci.*, 2017, **418**, 328–334.

